

The Transition between Tonic Spiking and Bursting in a Six-Transistor Neuromorphic Device

Fernando Castaños

Centro de Investigación y de Estudios Avanzados
Instituto Politécnico Nacional, México
Email: castanos@ieee.org

Alessio Franci

Universidad Nacional Autónoma de México
Facultad de Ciencias
Email: afranci@ciencias.unam.mx

Abstract—We introduce a novel methodology to implement the physiological transition between tonic spiking and bursting in electronic circuits composed of resistors, capacitors and transistors. The result is a six-transistor neuromorphic device organized by the same geometry of high-dimensional electrophysiological neuron models and therefore exhibiting the same qualitative behavior.

I. INTRODUCTION

Nature offers spectacular examples of energy-efficient, lightweight control architectures. Flight control in a simple animal like a honeybee outperforms the latest robotic architectures in terms of energy consumption, adaptability, robustness, and dimensions. Neuromorphic engineering aims at emulating the way in which biological neuronal systems perceive and represent the outside world, take decisions and develop computations, and command motor outputs [1], [2].

In implementing the dynamical behavior of biological neurons in electronic hardware we face the compromise between fidelity of the reproduced behavior and complexity of the designed circuit. Existing silicon neuron designs span a variety of solutions: from detailed implementation of neuron biophysics [3] to implementation of simple, abstract neuron models [4]. Both approaches have advantages and disadvantages, and it is an active research area to determine which implementation to use depending on the desired objective [5].

The possibility of reliably and rapidly switching between distinct dynamical modes is one of the peculiarity of biological neurons, which allows them to adapt their input-output response depending on internal and environmental conditions. Two fundamental neuronal activity modes are tonic spiking and bursting. Tonic spiking describes the slow, regular generation of spikes in the neuron membrane potential. Bursting describes the alternation between moments of low membrane potential and moments of high oscillatory activity, in which spikes are generated at very high frequency. The transition between tonic spiking and bursting plays a major role in the processing of sensory information [6], [7].

We showed [8], [9] that all biological neurons share the same geometry for the transition between tonic spiking and bursting. In particular, this transition can be described in a simple, abstract model given by the normal form of an organizing singularity. Roughly speaking, a singularity describes a highly degenerate and fragile situation that correspond

to the transition between distinct regimes [10]. There is a direct correspondence between biophysical parameters and mathematical parameters in the abstract model, which leads to a profound mathematical understanding of robustness and modulation of neuronal activity [11]. We further showed that the same qualitative picture can be realized in simple circuits [12].

In this paper, we follow the recipe provided in [12] to design a neuromorphic circuit with the property of sharing the same qualitative geometry, robustness, and modulation capabilities of biophysical neuron models. As a first, biologically relevant exploration, we focus on the transition between tonic spiking and bursting. The resulting circuit solely uses six transistors and passive elements. For comparison, the simplest available neuromorphic circuit capable of transitioning between tonic spiking and bursting uses fourteen mosfet transistors [4]. Another advantage of our approach is that circuit parameters are constructively tuned by geometric inspection of its static input-output characteristic, which avoids laborious and non-constructive parameter fitting procedures.

In Section II we rapidly review the results in [8], [9], [12]. Grounded in these works, we derive an implementation of our neuromorphic device in Section III. The appendix contains the necessary code for simulating it.

II. THE GEOMETRY OF NEURONAL BURSTING AND ITS BLOCK REALIZATION

Electrophysiological models of neurons are constructed upon the seminal work of Hodgkin and Huxley [13]. They all share the physical interpretation of the nonlinear RC circuit depicted in Fig. 1-A. The capacitor models the neuron membrane and the other branches, containing a voltage source and a variable resistance, model the flow of a specific ion across the membrane.

Ion flow across the membrane is dynamically regulated by the membrane potential via opening and closing of the ion channels, which makes the circuit in Fig. 1-A highly nonlinear. As such, it can exhibit a rich variety of dynamical behaviors. The present paper focuses on two fundamental behaviors shared by almost all neuron types: the tonic spiking behavior of Fig. 1-B left and the bursting behavior of Fig. 1-B right.

Reproducing tonic spiking and bursting, as well as the transition between these two modes, in an electrophysiological

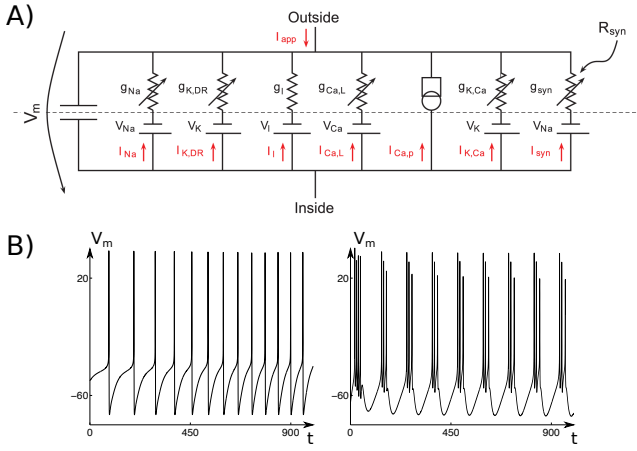


Fig. 1: A. The RC circuit associated to a conductance-based biophysical model of neuron. B. Two dynamical modes in a conductance-based model. Left: tonic spiking. Right: bursting. Membrane potential values are in millivolts. Time is in millisecond.

ical model requires a fine tuning of the many biophysical parameters that usually ends up in an extensive brute-force computational parameter search [14]. A different approach relies on bifurcation theory [15].

Roughly speaking, bifurcation theory makes the ansatz that the vector field associated to an electrophysiological model undergoes some qualitative change at the transition between two distinct dynamical modes.

We showed in [8], [9] that the bifurcation associated to the transition between tonic spiking and bursting can be algebraically tracked by exploiting the multi-timescale nature of electrophysiological neuron models and by detecting a transcritical singularity in the critical manifold of the associated singularly perturbed dynamics. We refer the reader to [16] for an introduction to geometric singular perturbation theory and to [10] for singularity theory concepts.

The power of this analysis is that we can visualize the geometry of the tonic spiking - bursting transition in a low-dimensional normal form of the organizing singularity:

$$\dot{x} = -x^3 - (\lambda + y)^2 + \beta x - \alpha - z \quad (1a)$$

$$\dot{y} = \varepsilon_s(x - y) \quad (1b)$$

$$\dot{z} = \varepsilon_u(x - z), \quad (1c)$$

where λ is called the bifurcation parameter, α, β are called unfolding parameters, and $0 < \varepsilon_u \ll \varepsilon_s \ll 1$ model timescale separation between the three state variables x , y and z . The distinction between bifurcation and unfolding parameters is instrumental to the tools used in the construction of the normal form (1), that is, singularity theory applied to bifurcation problems [10].

Fig. 2-A shows the temporal traces and the projection onto the phase plane of the slow-fast subsystem (1a-1b) of tonic spiking and bursting behaviors in model (1). It shows that,

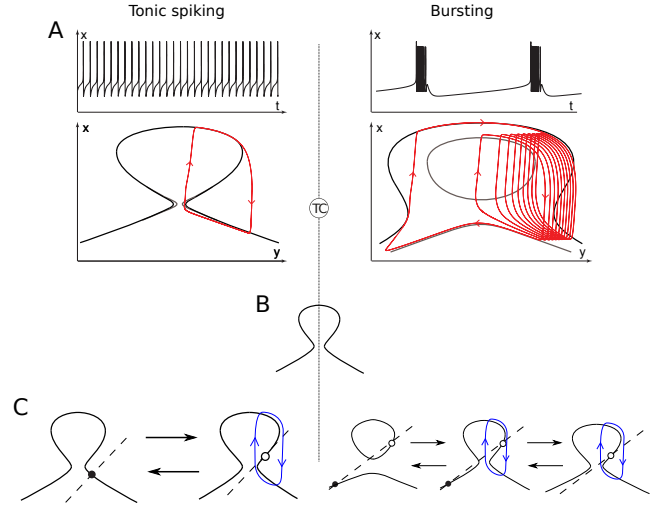


Fig. 2: A. Top: temporal traces of mode (1) in tonic spiking and bursting. Bottom: projection of the trajectory on the $x - y$ phase plane. The trajectory is in red. The critical manifold (2) is black for small value of z and in gray for large value of z . B. The mirrored hysteresis bifurcation diagram. C. The geometry of tonic spiking and bursting. The black dot denotes stable fixed point, the circle unstable fixed points. Stable limit cycles are drawn in blue.

due to timescale separation, trajectories spend most of the time near the critical manifold

$$\mathcal{Z} := \{(x, y, z) \in \mathbb{R}^3 : \dot{x} = 0\}, \quad (2)$$

that is, the x -nullcline composed of x steady states as y and z varies.

The fundamental shape of the critical manifold underlying the transition between tonic spiking and bursting is the mirrored hysteresis bifurcation diagram introduced in [9] and sketched in Fig. 2-B. In the tonic spiking mode trajectories solely visits the right branch of the mirrored hysteresis, whereas in bursting mode trajectories alternate between the two branches.

The geometry of both behaviors is sketched in Fig. 2-C. In tonic mode, for each value of the ultra-slow variable z , the slow-fast subsystem possesses a single attractor on the right branch of the mirrored hysteresis: either a stable fixed point, for large value of z (left plot), or a stable limit cycle, for small value of z (right plot). For large initial values of z the model is therefore at quasi-steady state. The ultraslow dynamics (1c) lets in this case z decrease until the steady state loses stability and a spike is emitted along the newborn limit cycle. This in turn leads to a sharp increase of z , which immediately lets the steady state recover stability, and the model is forced back to quasi-steady state.

In bursting mode, there exists a large range of values of the ultraslow variable z in which the slow-fast subsystem exhibits bistability between a stable steady state on the left branch of the mirrored hysteresis and a limit cycle on the right branch of the mirrored hysteresis (center plot). For large

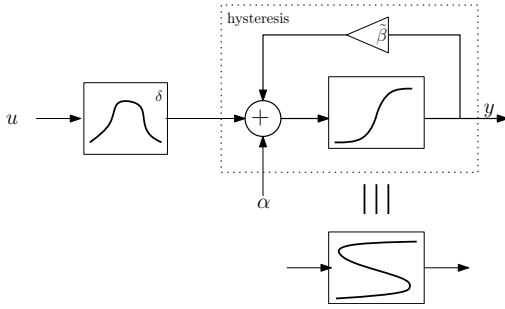


Fig. 3: Block realization of a mirrored hysteresis nonlinear characteristic.

initial value of z the sole attractor is a stable steady state (left plot). The ultraslow dynamics (1c) lets in this case z decrease. However, once in the bistable region, the model remains at quasi-steady state. Only for sufficiently large z the steady state loses stability and the trajectory converges toward the spiking limit cycle, which is now the sole attractor (left plot). On the limit cycle (1c) lets z decrease. Again, all through the bistable region the system remains in the oscillatory mode and only for z sufficiently large the trajectory converges to its quasi-steady state.

Normal forms are useful not only because they unmask the geometry underlying a given dynamical behavior, but also because they possess the minimum number of parameters to reproduce a family of behaviors of interest. As such they can also be implemented in physical devices much more easily and robustly than the original biophysical model, yet, preserving the same geometric and input/output properties.

We showed in [12] that the mirrored hysteresis bifurcation diagram can be realized in the input-output diagram of Fig. 3. Its basic ingredients are a non-monotone nonlinearity cascaded with a saturation nonlinearity and a positive feedback loop around the saturation nonlinearity. The positive feedback loop transforms the saturation into a hysteresis [12, Proposition 1], the non-monotone block creates a mirror of the resulting hysteretic characteristic.

Adding linear dynamical systems evolving on three sharply different timescales (Fig. 4) transforms the static circuit in Fig. 3 into a three-timescale dynamical system with the same qualitative behavior of model (1). In particular, the circuit in Fig. 4 exhibits the same geometric transition between tonic spiking and bursting as model (1).

III. ELECTRONIC IMPLEMENTATION

In this section we derive an electronic implementation of the circuit in Fig. 4. The main active component is an npn transistor. Its constitutive relations are given by Ebers-Moll equations [17] but, to simplify the analysis, we will model the transistor as a current source with current proportional to that of a diode standing at the base. Furthermore, will regard the diode as a perfect switch that opens whenever $v_{BE} \geq 0.6$ and closes otherwise.

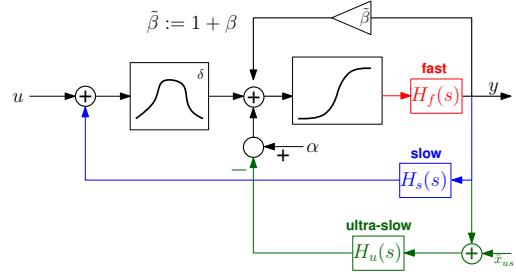


Fig. 4: Block realization of a neuron model. The linear filters $H_{f,s,u}(s)$ are first order filters with sharply separated cut-off frequency: large for H_f , intermediate for H_s , and small for H_u .

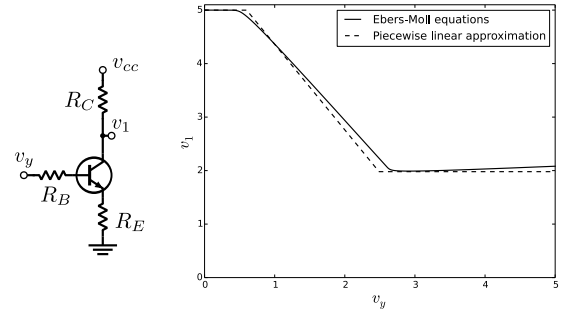


Fig. 5: Basic saturation. Common-emitter configuration (left). Piecewise linear approximation vs. exact solutions (right).

A. Voltage-controlled non-monotone characteristic

The non-monotone block of the circuit in Fig. 4 is realized as the difference of two monotone nonlinearities [12]. A common emitter npn transistor configuration serves as a simple, natural saturation monotone nonlinearity (see Fig. 5). In view of the transistor model described above, the v_y-v_1 characteristic takes the piecewise linear form

$$v_1 = v_{cc} - \text{Proj}_{S_1}(g_1(v_y - 0.6)), \quad (3)$$

where

$$g_1 = \frac{\beta R_C}{R_B + (\beta + 1)R_E}$$

is the voltage gain (the slope of the saturation), $\beta \approx 100$ is the transistor's current gain and $S_1 = [0, v_s]$ with

$$v_s = (v_{cc} - 0.1) \frac{R_C}{R_C + R_E}$$

the saturation voltage. Usually, one chooses $R_B \ll \beta R_E$ so that $g_1 \approx \frac{R_C}{R_E}$, that is, so that the dependence of g_1 on β is negligible. The operator Proj_{S_1} projects its argument into the set S_1 , that is, $\text{Proj}_{S_1}(v) = \text{argmin}_{w \in S_1} \|v - w\|$. For our particular S_1 , the projection translates into

$$\text{Proj}_{S_1}(v) = \begin{cases} 0 & \text{if } v \leq 0 \\ v & \text{if } 0 \leq v \leq v_s \\ v_s & \text{if } v_s \leq v \end{cases}.$$

To assess the quality of our estimation, we choose a set of parameters and compare (3) against the simulation obtained

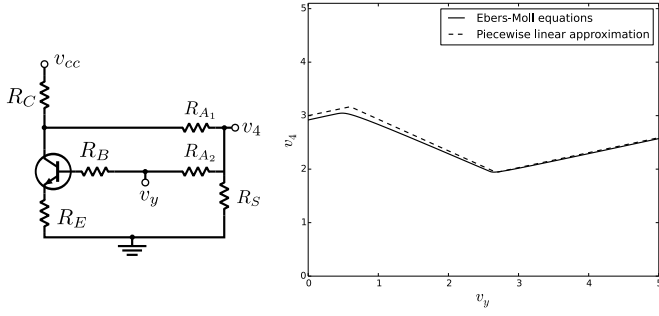


Fig. 6: Non monotone characteristic. Parallel interconnection of a saturation and a linear gain (left). Piecewise linear approximation vs. exact solutions (right).

using `ngspice` (which implements Ebers-Moll equations). The results are shown in Fig. 5.

The parallel interconnection achieving the non-monotone behavior is shown in Fig. 6, left. Applying Kirchhoff's laws and the piecewise linear model for the transistor one obtains

$$v_4 = g_2(v_{cc} - \text{Proj}_{S_1}(g_1(v_y - 0.6))) + g_3v_y \quad (4)$$

with

$$g_2 = \frac{R_S R_{A_2}}{R_S (R_{A_1} + R_{A_2}) + R_{A_1} R_{A_2}}$$

$$g_3 = \frac{R_S R_{A_1}}{R_S (R_{A_1} + R_{A_2}) + R_{A_1} R_{A_2}}$$

(see Fig. 6, right).

The characteristic (4) is non-monotone whenever strict extrema are present. A necessary condition for the presence of extrema is $0 \in \partial v_4$ [18, p. 70], where ∂v_4 is the subdifferential [18, p. 32] of v_4 with respect to v_y . For (4) we have $\partial v_4 = g_3 - g_1 g_2 \Psi_{S_1}(g_1(v_y - 0.6))$, where

$$\Psi_{S_1}(v) = \begin{cases} 0 & \text{if } v \notin S_1 \\ [0, 1] & \text{if } v \in \partial S_1 \\ 1 & \text{if } v \in \text{int } S_1 \end{cases}$$

with $\text{int } S_1$ and ∂S_1 the interior and the boundary of S_1 , respectively. Thus, $0 \in \partial v_4$ implies $g_1 > g_3/g_2$.

Let us compute some points of interest of the characteristic (4) (the computation of such points is useful for choosing the appropriate resistors):

$$v_4(0) = g_2 v_{cc}$$

$$v_4(0.6) = g_2 v_{cc} + g_3 0.6 \quad (\text{a local maximum})$$

$$v_4\left(\frac{v_s}{g_1}\right) = g_2 v_{cc} - \left(g_2 - \frac{g_3}{g_1}\right) v_s \quad (\text{a local minimum})$$

$$v_4(v_{cc}) = (g_2 + g_3)v_{cc} - g_2 v_s$$

(local extrema are found by solving $0 \in \partial v_4(v_y)$).

The possibility to modulate the non-monotone characteristic is achieved by cascading a differential amplifier as the one shown in Fig. 7, left. Kirchhoff's laws together with the piecewise linear model give

$$v_5 = v_{cc} - \text{Proj}_{S_2}(g_4(v_4 - 0.6) - g_5(v_z - 0.6)) \quad (5)$$

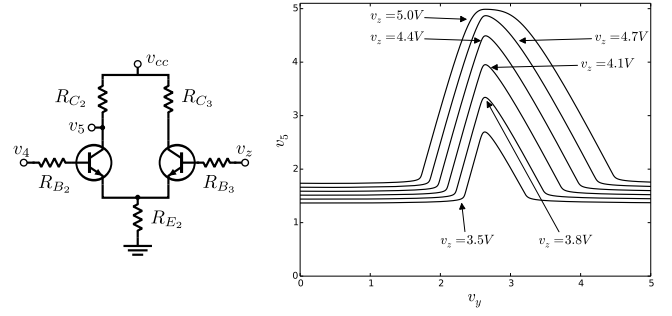


Fig. 7: The voltage-controlled non-monotone characteristic is realized by cascading a differential amplifier (left) with a fixed non-monotone characteristic (see Fig. 6). Input-output response for different values of v_z (right).

where

$$g_4 = \frac{\bar{R}_{C_1} (\bar{R}_E + R_{B_2})}{\bar{R}_E (R_{B_1} + R_{B_2}) + R_{B_1} R_{B_2}}$$

$$g_5 = \frac{\bar{R}_{C_1} \bar{R}_E}{\bar{R}_E (R_{B_1} + R_{B_2}) + R_{B_1} R_{B_2}}$$

$\bar{R}_C = (\beta + 1)R_C$ and $\bar{R}_E = (\beta + 1)R_E$. The voltage v_4 is the non-inverting input and v_z the inverting one. The complete block is shown in Fig. 11 and the input-output characteristic is shown in Fig. 7, right.

B. Hysteretic characteristic

The hysteretic block is built as the positive feedback of a basic saturation and a linear gain [12]. This is achieved at once with a differential amplifier like the one shown in Fig. 7, left. By letting v_5 be the inverting input, v_6 the non-inverting input and v_x the output, we obtain (cf. (5))

$$v_x = v_{cc} - \text{Proj}_{S_3}(g_6(v_5 - 0.6) - g_7(v_6 - 0.6)) \quad .$$

Positive feedback is then achieved simply by setting $v_6 = v_x$, as shown in Fig. 11. This results in the piecewise linear characteristic

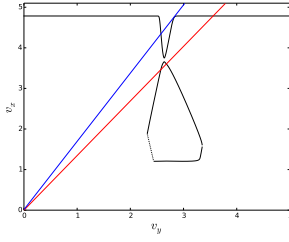
$$F(v_5, v_x) = v_x - v_{cc} + \text{Proj}_{S_3}(g_6(v_5 - 0.6) - g_7(v_x - 0.6)) = 0 \quad (6)$$

It follows from the implicit function theorem [19, p. 256] that a necessary condition for the existence of singular points is $0 \in \partial F(v_5, v_x)$ with the subdifferential taken with respect to v_x . For (6) we have

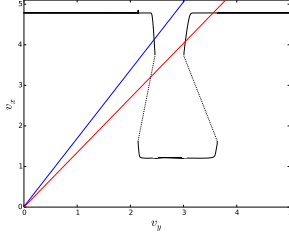
$$\partial F(v_5, v_x) = 1 - g_7 \Psi_{S_3}(g_6(v_5 - 0.6) - g_7(v_x - 0.6)) \quad ,$$

so that $0 \in \partial F(v_5, v_x)$ implies $g_7 > 1$. There are two points of singularity. The first one is characterized by $g_6(v_5 - 0.6) = g_7(v_x - 0.6)$ which, together with the condition $F(v_5, v_x) = 0$, gives

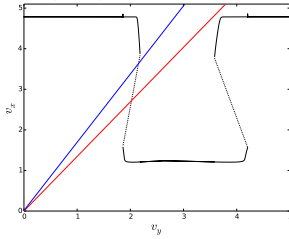
$$v_x = v_{cc} \quad \text{and} \quad v_5 = \frac{g_6}{g_7} v_{cc} + \frac{g_6 - g_7}{g_6} 0.6 \quad .$$



(a) $v_z = 3.8V$. A saddle point, an unstable and a stable node are present (red). A stable node is present (blue). In both cases, almost all trajectories converge to the stable node.



(b) $v_z = 4.1V$. A saddle point, a stable limit cycle around an unstable node and a stable node coexist (red). The only attractor is a stable node (blue).



(c) $v_z = 4.7V$. A stable limit cycle around an unstable node exists. Almost all trajectories converge to the limit cycle (red and blue).

Fig. 8: Mirrored-hysteresis. Solid black lines correspond to the x -steady states found by solving the circuit with `ngspice`. Dotted lines are manually added to sketch the solutions not found by the solver. Red and blue lines correspond to the desired v_y -nullclines.

The other point of singularity is determined by $g_6(v_5 - 0.6) = g_7(v_x - 0.6) + v_s$, which gives

$$v_x = v_{cc} - v_s \quad \text{and} \quad v_5 = \frac{g_7}{g_6} v_{cc} + \frac{g_6 - g_7}{g_6} 0.6 - \frac{g_7 - 1}{g_6} v_s.$$

C. Voltage-controlled mirrored hysteresis

The cascade of the controlled non-monotone block and the hysteresis (see Fig. 11) produces the desired voltage-controlled mirror hysteresis (see Figs. 8a-8c, black). This characteristic is qualitatively equivalent to Figs. 2-C.

D. Burster

We now transform the static circuit in Fig. 11 into a dynamic circuit exhibiting the same qualitative dynamics as model (1).

The parasitic capacitances of the transistors provide the fast v_x dynamics and set its corresponding time-scale (cf. H_f in

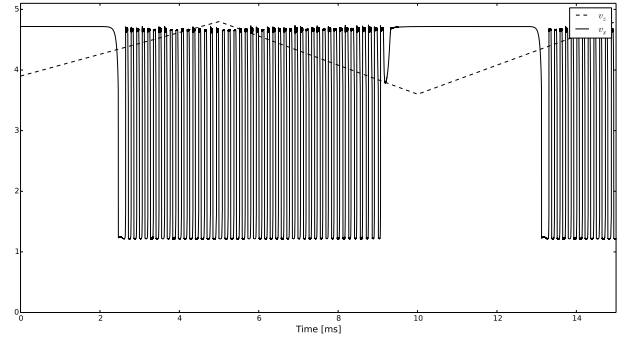


Fig. 9: Transition between a stable node (constant output) and a stable limit cycle (oscillations). The transitions occur at different values of v_z , which indicates that the stable node and the stable limit cycle coexist for some values of v_z .

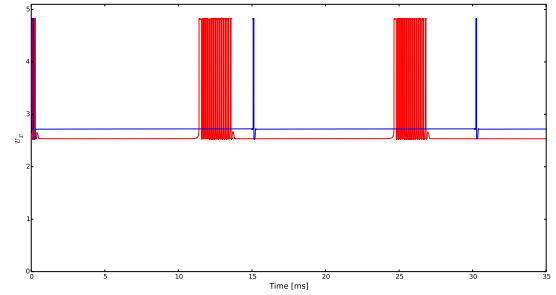


Fig. 10: Bursting (red) and spiking (blue).

Fig. 4). The voltage v_x is fed back to v_y by means of a resistive voltage divider and a capacitor. The values of the resistors and the capacitor determine the time-scale of the slow v_y dynamics as well as the slope of its nullcline (cf. H_s in Fig. 4).

Figs. 8a-8c confirm the qualitative equivalence of the circuit in Fig. 11 and model (1). By sweeping v_z we recover the same qualitative phase portraits of Fig. 2-C left, which underlie the behavior simulated in Fig. 9. A key ingredient in the bursting behavior is the bistability of the limit cycle and the node (Fig. 8b, red). The presence of this phenomenon can be asserted by noting that the transition from the constant output (the stable node) to the oscillating behavior (the limit cycle) occurs at a higher value of v_z than the one for the transition from the oscillating behavior to the constant output.

Bursting is finally achieved by feeding v_x back to v_z through the ultra slow filter H_u . This is again realized with a voltage divider and a capacitor, but now the circuit's time-constant is chosen much larger. To ensure a robust operation, the output of H_u is amplified so that v_z exhibits a large swing. In fact it is the complement of v_x that is passed through an amplifier with negative slope (this accounts for the sixth transistor). The time response is shown in Fig. 10.

E. Spiker

Recall that the mirrored hysteresis captures both modes of operation: bursting and tonic spiking. Geometrically, the difference between the two behaviors is the locus of the stable fixed point, as sketched in Fig. 2. In our circuit, we recover

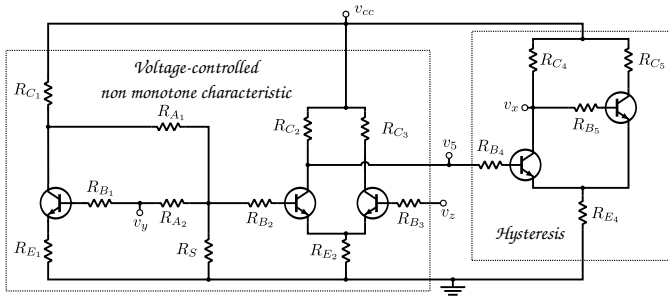


Fig. 11: Circuit realizing the mirrored hysteresis. By suitably changing v_z , the v_y-v_x characteristic can adopt the three forms portrayed on Figs. 8a-8c (cf. the right part of Fig. 2).

the same geometric picture by changing the slope of the v_y -nullcline via tuning of the resistance R_{i_1} and R_{i_2} . When the slope of the v_y nullcline is sufficiently large this line solely intersects the left branch of the mirrored hysteresis (see Figs. 8b and 8c, blue), thus destroying the possibility of bistability underlying bursting. The model is in this case in the tonic spiking mode shown in Fig. 10.

IV. CONCLUSION AND PERSPECTIVES

We have implemented the biological transition between tonic spiking and bursting in a compact six-transistor model. This model can be used as the building block of neuromorphic sensory and computing devices. Future work will aim at further ameliorating the circuit, at an efficient hardware implementation, and at the assembly of small, medium, and large networks implementing different biological functions, from central pattern generation to attention control.

REFERENCES

[1] K. Boahen, "Neuromorphic microchips," *Scientific American*, vol. 292, no. 5, pp. 56–63, 2005.

[2] S.-C. Liu and T. Delbruck, "Neuromorphic sensory systems," *Current opinion in neurobiology*, vol. 20, no. 3, pp. 288–295, 2010.

[3] K. M. Hynna and K. Boahen, "Thermodynamically equivalent silicon models of voltage-dependent ion channels," *Neural Computation*, vol. 19, no. 2, pp. 327–350, 2007.

[4] J. H. Wijekoon and P. Dudek, "Compact silicon neuron circuit with spiking and bursting behaviour," *Neural Networks*, vol. 21, no. 2, pp. 524–534, 2008.

[5] G. Indiveri, B. Linares-Barranco, T. J. Hamilton, A. Van Schaik, R. Etienne-Cummings, T. Delbruck, S.-C. Liu, P. Dudek, P. Häfliger, S. Renaud *et al.*, "Neuromorphic silicon neuron circuits," *Frontiers in neuroscience*, vol. 5, 2011.

[6] R. Krahe and F. Gabbiani, "Burst firing in sensory systems," *Nature Reviews Neuroscience*, vol. 5, no. 1, pp. 13–23, 2004.

[7] S. S. Sherman and R. W. Guillery, *Exploring the thalamus*. Oxford Univ Press, 2001, vol. 312.

[8] A. Franci, G. Drion, V. Seutin, and R. Sepulchre, "A balance equation determines a switch in neuronal excitability," *PLoS Computational Biology*, 2013.

[9] A. Franci, G. Drion, and R. Sepulchre, "Modeling the modulation of neuronal bursting: a singularity theory approach," *SIAM Journal on Applied Dynamical Systems*, vol. 13, no. 2, pp. 798–829, 2014.

[10] D. G. Schaeffer and M. Golubitsky, "Singularities and groups in bifurcation theory," *Appl. Math. Sci.*, vol. 51, 1985.

[11] G. Drion, A. Franci, J. Dethier, and R. Sepulchre, "Dynamic input conductances shape neuronal spiking," *eneuro*, vol. 2, no. 2, pp. ENEURO-0031, 2015.

[12] A. Franci and R. Sepulchre, "Realization of nonlinear behaviors from organizing centers," in *Proc. Conference on Decision and Control*, Los Angeles, CA, Dec. 2014, pp. 56 – 61. [Online]. Available: singularity/franci2014.pdf

[13] A. L. Hodgkin and A. F. Huxley, "A quantitative description of membrane current and its application to conduction and excitation in nerve," *The Journal of physiology*, vol. 117, no. 4, pp. 500–544, 1952.

[14] A. A. Prinz, C. P. Billimoria, and E. Marder, "Alternative to hand-tuning conductance-based models: construction and analysis of databases of model neurons," *Journal of Neurophysiology*, vol. 90, no. 6, pp. 3998–4015, 2003.

[15] J. Guckenheimer and P. Holmes, *Nonlinear oscillations, dynamical systems, and bifurcations of vector fields*. Springer Science & Business Media, 1983, vol. 42.

[16] C. K. R. T. Jones, "Geometric singular perturbation theory," in *Dynamical systems*. Springer, 1995, pp. 44–118.

[17] A. S. Sedra and K. C. Smith, *Microelectronic Circuits*. New York: Oxford University Press, 2004.

[18] M. M. Mäkelä and P. Neittaanmäki, *Nonsmooth optimization*. Singapore: World Scientific, 1992.

[19] F. H. Clarke, *Optimization and Nonsmooth Analysis*. New York: Society for Industrial and Applied Mathematics, 1990.

APPENDIX

```
Ngspice code for the complete circuit
* this is complete.cir file
* voltage resources
vcc 5 0 dc 5V
* non monotone
q1 2 3 4 2n2222bis
rC1 5 2 16k
rB1 3 1 100k
rE1 4 0 10k
Ra1 6 1 100k
Ra2 6 2 33k
Rs 6 0 220k
* non monotone modulation
q2 7 8 9 2n2222bis
q3 10 11 9 2n2222bis
rC2 7 5 4.7k
rC3 10 5 4.7k
rB2 8 6 1k
rB3 12 11 1.2k
rE2 9 0 470
* hysteresis
q4 13 14 15 2n2222bis
q5 16 17 15 2n2222bis
rC4 13 5 820
rC5 16 5 240
rB4 14 7 2.4k
rB5 17 13 6k
rE4 15 0 240
* vy-vx feedback loop
ri1 13 1 15k
ri2 1 0 47k
* Set ri2 to 34.5k for tonic spiking
ciF 1 0 22n
* vz-vx feedback loop
q6 12 18 19 2n2222bis
ro1 16 18 4.7k
ro2 18 0 4.7k
coF 18 0 4.7u
rC6 12 5 200
rE6 19 0 20
rbi 19 5 150
* model for a 2n2222 transistor
.model 2n2222bis npn (is=14.34f bf=255.9 vaf=74.03 ikf=.2847
+ ise=14.34f ne=1.307 br=6.092 ikr=0 isc=0 nc=2 rb=10
+ rc=1 cje=22.01p tf=411.1p cjc=7.306p tr=46.91n xtb=1.5
+ Xti=3 Eg=1.11 Mjc=.3416 Vjc=.75 Fc=.5 Mje=.377 Vje=.75
+ Itf=.6 Vtf=1.7 Xtf=3 )
.control
tran lus 40ms
plot v(16) ylimit 0 5
.endc
.end
```